HHS Public Access

Author manuscript

J Neuroimmunol. Author manuscript; available in PMC 2015 June 30.

Published in final edited form as:

J Neuroimmunol. 2014 June 15; 271(0): 18–29. doi:10.1016/j.jneuroim.2014.03.008.

Involvement of calcitonin gene-related peptide and receptor component protein in experimental autoimmune encephalomyelitis

Claudia Sardi[a,1], **Laura Zambusi**[a,b], **Annamaria Finardi**[c], **Francesca Ruffini**[c], **Adviye A. Tolun**[d,2], **Ian M. Dickerson**[e], **Marco Righi**[a,b], **Daniele Zacchetti**[c], **Fabio Grohovaz**[c,f], **Luciano Provini**[g], **Roberto Furlan**[c], and **Stefano Morara**[a,b,*]

Stefano Morara: stefano.morara@in.cnr.it

[a]Neuroscience Institute, C.N.R., Via Vanvitelli 32, 20129 Milano, Italy

[b]Dept. of Medical Biotechnol. Translational Medicine, University of Milano, Via Vanvitelli 32, 20129 Milano, Italy

[c]Division of Neuroscience, San Raffaele Scientific Institute, Via Olgettina 60, 20132 Milano, Italy

[d]Dept. of Biochem. Mol. Biol., University of Miami, Miami, FL 33101, USA

[e]Dept. of Neurobiol. Anatomy, University of Rochester, 601 Elmwood Avenue, Box 603, Rochester, NY 14642, USA

[f]Vita-Salute San Raffaele University, Via Olgettina 58, 20132 Milano, Italy

[g]Dept. of Pharmacol. Biomol. Sci., University of Milano, Via Trentacoste 2, 20133 Milano, Italy

Abstract

Calcitonin Gene-Related Peptide (CGRP) inhibits microglia inflammatory activation in vitro. We here analyzed the involvement of CGRP and Receptor Component Protein (RCP) in experimental autoimmune encephalomyelitis (EAE).

Alpha-CGRP deficiency increased EAE scores which followed the scale alpha-CGRP null > heterozygote > wild type. In wild type mice, CGRP delivery into the cerebrospinal fluid (CSF) 1) reduced chronic EAE (C-EAE) signs, 2) inhibited microglia activation (revealed by quantitative shape analysis), and 3) did not alter GFAP expression, cell density, lymphocyte infiltration, and peripheral lymphocyte production of IFN-gamma, TNF-alpha, IL-17, IL-2, and IL-4.

RCP (probe for receptor involvement) was expressed in white matter microglia, astrocytes, oligodendrocytes, and vascular-endothelial cells: in EAE, also in infiltrating lymphocytes. In relapsing–remitting EAE (R-EAE) RCP increased during relapse, without correlation with lymphocyte density. RCP nuclear localization (stimulated by CGRP in vitro) was I) increased in

*Corresponding author at: Neuroscience Institute, C.N.R., Via Vanvitelli 32, 20129 Milano, Italy. Tel.: +39 02 50317119; fax: +39 02 50316941.

[1]Present address: Humanitas Clinical and Research Center, Via Manzoni 56, Rozzano, Milano, Italy.

[2]Present address: Laboratory Corporation of America, Center for Molecular Biology and Pathology, 1912 T.W. Alexander Drive, RTP, NC 27709, USA.

Supplementary data to this article can be found online at http://dx.doi.org/10.1016/j.jneuroim.2014.03.008.

microglia and decreased in astrocytes (R-EAE), and II) increased in microglia by CGRP CSF delivery (C-EAE). Calcitonin like receptor was rarely localized in nuclei of control and relapse mice. CGRP increased in motoneurons.

In conclusion, CGRP can inhibit microglia activation in vivo in EAE. CGRP and its receptor may represent novel protective factors in EAE, apparently acting through the differential cell-specific intracellular translocationof RCP.

Keywords

Neuropeptides; Neuroinflammation; CSF delivery; Microglia; Quantitative image analysis; Nuclear localization

1. Introduction

Calcitonin Gene-Related Peptide (CGRP), a peptide generated from tissue-specific alternative splicing of the calcitonin gene (Amara et al., 1982), and adrenomedullin (Kitamura et al., 1993) are two homologous neuropeptides that signal through a common core G-protein-coupled receptor named Calcitonin-Like Receptor (CLR, Chang et al., 2004). However, CLR is an unusual G-protein-coupled receptor since it requires accessory proteins for its function. Three single-transmembrane accessory proteins have been identified and named Receptor Activity Modifying Proteins (RAMPs) 1–3. CLR is a high-affinity receptor for CGRP when co-expressed with RAMP1, and for adrenomedullin when co-expressed with RAMP2 or RAMP3 (McLatchie et al., 1998). These receptor complexes interact with an additional cytoplasmic protein, the CGRP-Receptor Component Protein (RCP), which is the functional link with the intracellular signaling pathways and, in particular, with cAMP formation (Evans et al., 2000; Egea and Dickerson, 2012).

CGRP and adrenomedullin can modulate both neural and immune systems. CGRP is expressed mainly by neuronal cells and promotes astrocytic and neuronal differentiation (D'Antoni et al., 2010) and modulates the activity of glial cells (Uezono et al., 2001; Wang et al., 2009). CGRP not only promotes neurogenic inflammation in the periphery (Holzer, 1998) and brain (during headache; Durham, 2006), but also protects against inflammatory injuries, as in LPS-induced local acute inflammation (Gomes et al., 2005) or immune-mediated liver injury (Kroeger et al., 2009). In addition, CGRP can directly induce the secretion of a variety of cytokines (IL-2, IFN-gamma, IL-4, IL-10 and TNF-alpha) from T cells (Levite, 1998) and regulate immune cell function, e.g., it can bias Langerhans cells toward Th-2 type immunity (Ding et al., 2008). CGRP can inhibit pre-B cell colony formation stimulated by IL-7 (Fernandez et al., 2000), LPS-induced kappa light chain expression in B lymphocytes (McGillis et al., 1993) and mitogen-stimulated T lymphocyte proliferation (Umeda et al., 1988). Finally, a study on RAMP1 knockout mice suggested that CGRP might produce both pro-and anti-inflammatory effects (Tsujikawa et al., 2007). Adrenomedullin is reported to exert pro-inflammatory roles (Clementi et al., 2000; Wong et al., 2005; Ma et al., 2006), but there is growing evidence of its protective anti-inflammatory roles in experimental models of diseases, such as pulmonary injury, hemorrhagic or septic shock, colitis, ischemia–reperfusion or arthritis (von der Hardt et al., 2002; Ashizuka et al.,

2005; Cui et al., 2005; Wu and Wang, 2006; Carrizo et al., 2007; Dackor and Caron, 2007; Gonzalez-Rey et al., 2007). The emerging picture indicates that CGRP and adrenomedullin can exert either pro-inflammatory effect or anti-inflammatory effect in a highly regulated tissue-specific and stimulus-specific manner. However, most of the studies on their immune-inflammatory actions concerned peripheral structures. CGRP and adrenomedullin brain-restricted actions have been analyzed in headaches studies, but whether the action is restricted to sensory endings of brain vasculature or brain parenchyma has not yet been defined. We recently showed that both CGRP and adrenomedullin inhibit the secretion of pro-inflammatory mediators from activated microglia (Consonni et al., 2011), and in the current studies we have addressed the role of these peptides in neuroinflammation.

Multiple sclerosis, a demyelinating disease of the central nervous system (CNS), is thought to be autoimmune and typically associated with CNS inflammatory infiltrates composed of activated microglia, lymphocytes and macrophages (Lucchinetti et al., 2000). It has been hypothesized that primary inflammatory cytokines (TNF-alpha, IL-1beta, and IL-6) are locally released by infiltrating and resident cells and trigger the production of secondary inflammatory mediators such as chemokines, colony stimulating factors, and lipids. Adhesion molecules are also up-regulated on endothelial cells, thus favoring the recruitment and infiltration of leukocytes (Engelhardt and Ransohoff, 2005). The inflammatory response is usually further amplified by local interaction of T cells with CNS resident cells (Flugel et al., 2001), such as microglia and astrocytes. However, the full array of mechanisms influencing the interaction of the dysregulated immune response with neural cells is not yet known.

Since CGRP and adrenomedullin modulate neural and immune cell functions and are synthesized within CNS, it can be hypothesized that they can modulate immune–neural interactions within the CNS thereby influencing multiple sclerosis pathogenesis. To test for the effect of these neuropeptides on EAE, 1) we explored the effect of CGRP null mutation on experimental autoimmune encephalomyelitis (EAE; an accepted preclinical model of multiple sclerosis) pathogenesis, 2) we administered CGRP into the cerebrospinal fluid (CSF) of EAE wild type mice and 3) we correlated EAE course with the expression of CGRP and CGRP/adrenomedullin receptor (using RCP as a marker) in the brain.

2. Materials and methods

All efforts were made to minimize animal suffering and to reduce the number of mice to be used, in accordance with the principles of the NIH Institutional Animal Care and Use Committee Guidebook (2002). All the present experiments were carried out in accordance with the European Communities Council Directive 2010/63/EU and approved by the Italian Ministry of Health. The mice were purchased from Charles River Italia (Calco, LC). Upon arrival the mice were placed in individual, sterilized cages with unlimited access to sterilized water and food (vitamin/nutrient-enriched diet: code 4RF25 purchased from Mucedola, Milano, Italy). In each cage a sterilized paper towel was inserted to allow the mice to create a nest by shredding the towel. Cages were kept in a conventional, periodically disinfected room where access was restricted to personnel of the group involved in EAE experiments who carried hair cover, gloves, animal facility gown, surgical mask and shoe covers. If,

following EAE induction, animals showed difficulties in reaching the pellets or drinking water, wet pellets and an easily accessible water dish were placed at the cage bottom. If animals showed signs of severe suffering they were immediately sacrificed.

2.1. EAE induction

Chronic EAE (C-EAE) was induced in alpha-CGRP deficient 129S6 mice (Lu et al., 1999; n = 36; 13 wild type, WT; 12 alpha-CGRP deficient, KO; 11 heterozygote mice, HT). These mutant mice carry a targeted mutation of calcitonin/alpha-CGRP gene that affects only alpha-CGRP production leaving unaltered calcitonin production. C-EAE was induced by subcutaneous immunization with 300 μl of 200 μg Myelin Oligodendrocyte Glycoprotein $(MOG)_{35–55}$ (from Multiple Peptide System) in incomplete Complete Freund's Adjuvant (CFA) containing 8 mg/ml killed *Mycobacterium tuberculosis* (strain H37Ra; Difco). Pertussis toxin (Sigma) (500 ng) was injected on the day of the immunization and again two days later as described previously (Furlan et al., 2009). Body weight and clinical score (0 = healthy; 1 = limp tail; 2 = ataxia and/or paresis of hind limbs; 3 = paralysis of hind limbs and/or paresis of forelimbs; 4 = tetra paralysis; 5 = moribund or dead) were recorded daily. The score was assigned as the maximum value obtained among seven different tail and motor tests evaluated on a flat smooth surface (including righting reflex) or a grid (upside or underside). The evaluation of the clinical score was performed by reducing potential bias sources, i.e. by blinding and randomization: the operator was experimental group-blinded and the sequence of the animals was randomly changed daily by a second, experimental group-blinded operator. In a second experimental model C-EAE was induced in 7–8 week old C57BL/6 female mice for spinal CSF delivery of CGRP (see below) by using the same protocol. In these experiments 31 mice (four independent experiments; 16 control mice, 15 CGRP-treated mice; weight range = 20–21 g) were used.

Relapsing–remitting EAE (R-EAE) was induced in 7–8 week old SJL female mice (n = 14; three independent experiments; weight range = 18–20 g) by subcutaneous immunization with 300 μl of 200 μg $PLP_{139–151}$ (Espikem) emulsified in CFA (1:2) and killed *M. tuberculosis* (8 mg/ml; strain H37Ra; Difco). Pertussis toxin (500 ng; Sigma) was injected on the day of the immunization and again two days later. Clinical relapses were defined as the occurrence of a clinical score increase of at least 0.5 persisting for a minimum of three consecutive days. In relapsing–remitting EAE experiments, mice were classified as either relapsing (when sacrificed at the second relapse after the onset peak), or remitting (when sacrificed at the remission that followed the second relapse after the onset peak). Disease onset occurred at 12.75 (+/−0.71) (mean +/− st. dev.) days post immunization (dpi), maximum clinical score was 3.12 (+/−0.43), and relapse rate (mean number of relapses occurring in the period 0–30 dpi) was 1.25 (+/−0.46).

In all types of EAE experiments (C-EAE: EAE induction in CGRP null 129S6 mice and CSF CGRP delivery in C57BL/6 mice; R-EAE: EAE induction in SJL mice) 100% of mice developed EAE clinical signs, although with strain-specific scores. In R-EAE experiments (PLP immunized mice: n = 14) four mice were sacrificed to avoid suffering, and two were not analyzed due to non regular alternating relapsing–remitting phases (defined as above). For Alzet (®) experiments, see below.

2.2. CGRP spinal CSF delivery

2002 model Alzet (®) osmotic minipumps (mean flow rate = 0.5 μl/h; duration = 14 days) were filled with artificial cerebrospinal fluid (aCSF) (containing 148.2 mM NaCl, 3 mM KCl, 1.4 mM $CaCl_2$, 0.8 mM $MgCl_2$, 0.8 mM Na_2HPO_4, 0.2 mM NaH_2PO_4 and 0.1% Bovine Serum Albumin, BSA). For CGRP treatment, peptide concentration was 100 μM (mean CGRP administration rate = 50 pmol/h). Four independent experiments were performed (total mice number = 31). A poly-urethane mouse intrathecal catheter (tip diameter: 32 G = 0.23 mm OD; Alzet, ®) was connected to the pump flow moderator. Minipumps were primed overnight at room temperature in 0.9% NaCl. At 2 dpi, chronic EAE mice were deeply anesthetized with xylazine (10 mg/kg) and Zoletil (®) (40 mg/kg) and a small incision was performed to access L6 vertebra. Following laminectomy and dura incision, the catheter distal segment (7–8 mm long) was inserted in the cranial direction. The catheter was glued with dental cement to the vertebrae and the minipump inserted cranially in a paravertebral location. At sacrifice (16 dpi), catheter tip was generally detected at L3–L4 vertebrae level: at this level only the thin conus medullaris is present and no spinal cord compression and pial inflammation were produced. In order to allow for at least a partial post-surgical recovery, body weight and clinical score were recorded daily starting from 7 dpi. Blinding and randomization during clinical score evaluation were performed as described above. The statistical analysis of CGRP-treated vs control animals was performed by the non-parametric Mann–Whitney U test (see below). The first inclusion criterion for the statistical analysis was the development of EAE signs: all animals developed appropriate symptoms. In Alzet (®) experiments, however, four animals (out of 35 MOG immunized) were excluded due to 1) catheter tip extra dural location (one animal), 2) catheter throttling (one animal), and 3) death (two animals).

2.3. Histology and immunofluorescence

Mice were sacrificed by perfusion with 4% paraformaldehyde following deep general anesthesia with urethane, and the brains were embedded in sucrose, frozen and cut at the cryostat. Spinal cord sections for histology and immunofluorescence examination were prepared as previously described (Morara et al., 2000). In brief, following a short perfusion with 4% paraformaldehyde, the dissected spinal cords were postfixed for 30 min in the same fixative, soaked overnight in 20% sucrose at 4 °C, frozen, cut at cryostat in the coronal plane at 10μm thickness and collected on gelatin-coated slides. Immunofluorescence was performed as previously described (Morara et al., 2008). The following primary antisera/antibodies were used: RCP #1047 (1:100, rabbit polyclonal: directed against mouse $RCP_{127–140}$); CGRP (1:1000, rabbit polyclonal, Peninsula); CLR (1:600, rabbit polyclonal, Santa Cruz Biotechnology, sc-30028); adrenomedullin (1:1000, rabbit polyclonal, Peninsula). The following cell-specific markers were used: Texas Red-conjugated Tomato Lectin (TL) (1:100, Vector: microglia and endothelial cells) or Iba-1 (1/500 rabbit, Wako: microglia); GFAP (1:1500, monoclonal, Sigma: astrocytes); CNPase (1:300, mouse monoclonal, Chemicon: oligodendrocytes); CD3 (1:200, rat, Serotec: lymphocytes); MBP (1:200, rat, Chemicon: myelin); neurofilament (NF) 200 (1/400, mouse monoclonal, Sigma: axons). Secondary antisera included Alexa-Fluor 488-conjugated donkey antirabbit and Alexa-Fluor 594-conjugated goat anti-mouse (both 1:400; Molecular Probes). When mouse monoclonal antibodies were used sections were pre-incubated with Mouse Blocking kit

(Vector). No immunoreactivity was obtained when immunofluorescence control experiments were performed by 1) omission of primary antisera/antibodies or 2) preadsorption of antisera/antibodies by related peptides. It should be noted that disruption of normal spinal cord white matter parenchyma by EAE (e.g., in relapsing mice) could produce high levels of non-specific background staining (as evidenced by immunochemical experiments performed by omitting primary antibodies). This holds true particularly when anti-mouse antibodies were used, and in fact, Mouse Blocking kit usage has to be adjusted accordingly. DAPI staining was used to identify nuclei in RCP cell localization experiments.

For evaluation of CNS cell infiltration in lumbar CSF delivery experiments, images from hematoxylin/eosin stained sections were taken by a digital camera attached to an AxioPlan Zeiss microscope equipped with a 20× objective. Cell counts were performed on images taken from meninges and parenchyma (number of fields = 53–67/mice, randomly sampled from 35 sections/mice, spanning the whole spinal cord length; 3 mice/group; 2 groups: CGRP-treated, control). Number of cells was automatically calculated by the Foci Picker3D plugin (ImageJ software) (ImageJ is freeware from NIH, Bethesda, Maryland: http://imagej.nih.gov/ij/): the results were similar to those obtained by two unbiased, skilled operators that performed manual counting (not shown). Inflammatory infiltrates were evaluated as the number of cell per mm^2.

2.4. Confocal analysis

The analysis was performed by a LSM 510 Meta confocal microscope (Zeiss). Immunolabeled sections were examined with 63× (1.4 N.A.), 40× (1.3 N.A.) or 20× (0.45 N.A.) Zeiss objectives using triple excitation wavelengths (405 nmfor DAPI, 488 nmfor Alexa-Fluor 488 and 568 nm for Alexa-Fluor 594).

The changes of microglia morphology in CGRP lumbar CSF delivery experiments were analyzed by calculating the round values (ratio between minor and major axes of best fit ellipse) by a home-made ImageJ macro using built-in commands. In order to have reference points of the parameter for standardization, we compared microglia round values in naive and relapsing mice (see below for details). In both experiment types, confocal images were taken from Iba-1, GFAP and DAPI triple-stained spinal cord sections using 40× objective. In naive and relapsing mice, the standardization for microglia morphology was performed on 18–40 scans/mice (3 mice/group; 21–45 cells/mice): a total number of 79 cells and 101 cells were analyzed in naive and relapsing mice, respectively. In CGRP lumbar CSF delivery experiments 34–48 scans/mice were taken from twelve equally-spaced sections spanning the whole spinal cord length (5 mice/group; 2 groups): a total number of 978 cells and 1315 cells were analyzed in CGRP-treated and control mice, respectively. In each section, Z-series (12 planes, spacing = 1 μm) were taken from the ventro-medial, ventro-lateral, dorso-lateral and dorso-medial regions. Following median filtering, a threshold was applied to eliminate background. DAPI stained/Iba-1-positive objects were identified by colocalization in a 300 nm cytoplasmic ring around the nucleus within single focal planes.

For RCP and CLR cellular (40× objective) and intracellular (63× objective) localization quantitative analyses (in R-EAE and in C-EAE) we performed a triple labeling for RCP or CLR nuclei (by DAPI staining) and specific cell type markers (GFAP for astrocytes, TL for

microglia and endothelial cells, CNPase for oligodendrocytes) in the spinal cord. For RCP cellular analysis in R-EAE, confocal scans were randomly taken from white matter areas (mice number: n = 4 for each group: ctr, CFA, rem, rel; 16–67 scans/mice; scan numbers of control vs relapse: 212 vs 134 for microglia, 258 vs 101 for astrocytes, 47 vs 77 for oligodendrocytes) and analyzed by IN Cell Analyzer 1000 (GE Lifesciences). In the RCP intracellular localization analysis during R-EAE, the number of specific cell types of control vs relapse mice was 228 vs 945 microglia, 502 vs 533 astrocytes and 139 vs 416 oligodendrocytes, respectively. In the RCP intracellular localization analysis during C-EAE, the number of microglia was 95 cells and 83 cells in aCSF- and CGRP-treated mice, respectively. In the CLR intracellular localization analysis during R-EAE, the number of microglia was 50 cells and 136 cells in control and relapse mice, respectively. A threshold was applied to each channel to discard background. Following positive identification of a cell by the presence of DAPI staining, the presence of cell-specific marker staining in a 700 nm thick rim around nucleus allowed to identify each cell type. The identification of a cell as microglia or endothelial cell (both labeled by TL) was performed on the basis of nuclear size and shape (as revealed by DAPI staining) and TL staining intensity and shape. The thickness of the rim around the nucleus was chosen as the best compromise among resolution, signal-to-noise ratio of the cell-specific marker (hampered, e.g., by generally low expression of GFAP and TL around the nuclei of tissue astrocytes or ramified microglia, respectively) and avoidance of false positivity (e.g., caused by strongly labeled GFAP processes running close to eccentric nuclei of GFAP-negative cells). It should be noted that EAE induces strong changes in the expression of cell-specific markers. For example, it is well known that, just around lesion areas (identified by lymphocyte infiltration and/or demyelinization), GFAP is generally increased in relapse mice spinal cord white matter as compared to control mice and is further highly increased within lesion areas. In parallel, TL is expressed only at low levels in ramified microglia whereas in activated or ameboid/phagocytic microglia it attains very high expression levels. Finally, background levels are also significantly variable, being highest in lesion areas: indeed, a correlation analysis showed a strong linear association of background fluorescence (i.e., fluorescence obtained in immunochemical experiments in which primary antibodies were lacking) with cell density (Suppl. Fig. 1; $R = 0.6018$, $p < =4.586e-06$). Thus, scan and analysis parameters had to be optimized for local variations to achieve appropriate cell identification. For intracellular localization, RCP-expressing cells were assigned to one of the three classes: nuclear-, cytoplasmic- and nuclear + cytoplasmic-expressing cells. Membrane localization, if present, was assigned to cytoplasmic localization.

A densitometric quantitative analysis of RCP expression in relapsing– remitting EAE mice was also performed. The analysis was performed by a spinning disk confocal microscope (Ultraview, PerkinElmer) equipped with a Zeiss Axioskop epifluorescence microscope. Immunolabeled sections were examined with 40× (1.3 N.A.) Zeiss objectives. The analysis was conducted by scanning 8–9 regularly spaced areas/mice in the ventro-medial region of funiculus (3 mice/group; 4 groups: naive, CFA, remitting, relapsing) spanning the whole length of the spinal cord. This area was chosen because it was one of the most frequently infiltrated areas, thus being potentially well suited to highlight any difference among disease states. A threshold was applied to discard background. Experiments were performed by

processing three groups, each including one control, one CFA, one remitting and one relapsing mouse. Results were expressed as percentage of mean fluorescence intensity of the corresponding control. The mean fluorescence intensity of the controls was 0.36 (+/−0.20) fluorescence units. For quantitative analysis of CGRP in motoneurons and dorsal horn, and adrenomedullin in dorsal horn a similar approach was used. Analysis was restricted to control and relapse mice. The mean fluorescence intensities of the controls were 0.65 (+/−0.37) fluorescence units for CGRP in motoneurons, 2.05 (+/−0.81) for CGRP in dorsal horn and 0.72 (+/−0.10) for adrenomedullin in dorsal horn. The samples for RCP, CGRP and adrenomedullin densitometric analysis followed a normal distribution and the ANOVA-one-way analysis was used.

The analysis on the correlation between RCP expression and lymphocyte density was conducted on three remitting and three relapsing mice. Spinal cord sections were double-labeled for RCP and CD3 staining. In the white matter, 2–5 scans were taken randomly from each section (9–12 sections/mouse): a total number of 56 and 134 scans were used from remitting and relapsing mice, respectively, for regression analysis.

The analysis of GFAP expression in CGRP lumbar CSF delivery experiments was carried out by measuring the GFAP mean fluorescence intensity (after threshold application) in 23–49 randomly sampled images/mice (3 mice/group).

2.5. Cell isolation and in vitro proliferation assays

Single cell-suspensions were obtained from lymph nodes and spleens of untreated or treated mice (two independent experiments; CGRP-treated mice: n = 6, control mice: n = 8). Triplicate cultures of (2.5 × 105/well) CFSE-labeled (Invitrogen, Carlsbad, CA) cells were cultured in round-bottom 96-well culture plates (CoStar, Cambridge, MA) in HL1 medium, supplemented with 2% U-glutamine (Lonza, Belgium) and 50 μg/ml Gentamicin (Sigma, St Louis, MO) with serial concentrations 0, 1, 3, 10, and 20 μM of the $MOG_{35–55}$ peptide or precoated with plate-bound 2.5 μg/ml α-CD3 (clone 145-2C11) plus 5 μg/ml soluble α-CD28 (clone 37.51) mAbs (BD Biosciences, Mountain View, CA). After 72 h at 37 °C, samples were acquired on a FACSCanto (Beckman Coulter) and data were analyzed using FlowJo software (TreeStar, Ashland, OR) to assess cell proliferation.

2.6. ELISA cytokine assays

Lymph node cells and splenocytes were cultivated as above. Supernatants were collected after 48 h to assess IL-4 and IFN-gamma cytokine production by a mouse-specific ELISA (DuoSet) kit purchased from R&D Systems (UK) according to the manufacturer's protocol. Standards were assayed in duplicate and samples in triplicate.

2.7. TaqMan analysis

Whole brain RNA was extracted in TRIzol (Invitrogen). Residual DNA was removed by treatment with 1 U DNase per 1 μg RNA (RQ1 RNase-free DNase, Promega) at 37 °C for 30 min. cDNA synthesis from 3–5 μg total RNA was performed using Ready-To-Go You-Prime First-Strand Beads (Amersham Biosciences.) and Random Hexamer (New England Biolabs) according to the manufacturer's instructions. Adrenomedullin primers (Applied

Biosystems; Cat. #4331182) were used. The $2^{-\Delta\Delta CT}$ method was used to calculate relative changes in gene expression, using GAPDH values to normalize.

2.8. In vitro intracellular RCP analysis

NIH3T3 cells were grown in ` with 100 nM CGRP for the indicated times. Following incubation, cells were scraped into 0.1 M 2-(N-morpholino) ethanesulfonic acid, pH 6, supplemented with protease inhibitors (50 μg/ml lima bean trypsin inhibitor, 2 μg/ml leupeptin, 16 μg/ml benzamidine, 2 μg/ml pepstatin A, 60 μg/ml phenylmethylsulfonyl fluoride) and homogenized at high speed in a Brinkmann Polytron for 15 s, and incubated on ice for 30 min. Cell lysates were then centrifuged for 10 min at 700 ×*g*, and pellet (nuclear fraction) was saved on ice. Supernate from first centrifugation was then centrifuged for 60 min at 4° C at 100,000 ×*g* to isolate membranes (pellet) and cytoplasm (supernate). Protein concentration was determined for each fraction, and 30 μg of each fraction was separated by SDS-PAGE, transferred to Immobilon membrane, and probed with anti-RCP antibody R83 using methods previously described (Evans et al., 2000; Egea and Dickerson, 2012). The experiment was performed in triplicate.

2.9. Microglia preparation and transfection

Primary microglia was prepared according to Consonni et al. (2011) and a pCDNA3 expression plasmid encoding Venus-RCP was transfected by Lipofectamine 2000 (Life Technologies) following manufacturer's instructions. Quantification of Venus-RCP in the nucleus was performed by IN Cell Analyzer 1000 (GE Lifesciences).

2.10. Statistics

The analysis of EAE clinical score was carried out by Mann–Whitney U test (which is based on median values) since data are non-linear and require non-parametric analysis (see the guidelines for EAE experiments proposed by Baker and Amor, 2012). Other statistical analyses were performed by using Student's t test in case of two samples following a Gaussian (normal) distribution, ANOVA-one-way analysis in case of multiple samples following a Gaussian distribution or Wilcoxon rank-sum test (equivalent to Mann–Whitney U test) in case of two samples that did not follow a Gaussian distribution. The Gaussian distribution of the samples was checked by Jarque–Bera test, or by Lilliefors test in case of small samples.

3. Results

In a first chronic model, EAE was induced in alpha-CGRP deficient (KO) 129S6 mice (Lu et al., 1999). Wild type (WT) mice developed a mild form of EAE following injection of MOG35-55. The clinical score was followed up to 50 dpi to analyze the whole course of the disease (Fig. 1A). The cumulative clinical score, representative of the area under the curve and, in general, of disease burden, was significantly increased in alpha-CGRP deficient mice as compared to controls ($p = 0.0469$; Wilcoxon rank-sum test) (Fig. 1B). Differences were significant during the period of EAE development (up to peak: 1–17 dpi; $p = 0.0345$) and during the period that followed the peak, when a chronic (although mild) impairment was maintained (18–50 dpi; $p = 0.044$). In contrast, the clinical score of heterozygote EAE mice

(HT) did not differ significantly from controls (p = 0.3537). Interestingly, cumulative clinical scores followed the scale KO >HT >WT (Fig. 1B). At 50 dpi, no neuropathological alterations (lymphocyte infiltration or demyelinization) were detectable in spinal cord white matter of both wild type and alpha-CGRP deficient mice (not shown).

In a second chronic model (EAE induction in C57Bl/6 mice by $MOG_{35–55}$ immunization), CGRP was administered for two weeks (from 2 to 16 days post immunization, dpi) into lumbar spinal CSF. The onset of EAE sign detectability started around 13 dpi when the present protocol of immunization is applied (not shown; see Furlan et al., 2009 and Fig. 2A for a graphical representation). Since the treatment with CGRP lasts up to 16 dpi, the statistical analysis of the score was restricted to the last four days of treatment (13–16 dpi). During this period CGRP-treated mice showed a significant improvement of clinical score: the clinical score of CGRP-treated mice showed a delay and the cumulative score was significantly lower than control mice (p= 0.037; Mann–Whitney U test) (Fig. 2A–B). During this period median score values were 3.0 in control and 2.0 in CGRP-treated mice. Sham-treated (minipump-implanted) non-EAE mice (n = 4) displayed some mild signs at the tail and hind limbs due to the surgical trauma. Evaluated using the EAE score scale the median value was 1.5 (range 1.5–3) at the corresponding stage (11–14 dps).

To determine if CGRP effect was mediated by peptide leakage from CSF, we performed an immunological analysis taking advantage of the sensitivity of lymphocytes to direct CGRP stimulation. The analysis revealed that CGRP administration in the CSF of EAE mice was unable to influence lymphocyte production of interferon gamma, TNF-alpha, IL-17, IL-2, and IL-4 following nominal antigen (MOG) stimulation (Fig. 2C–G). Moreover, lymphocyte proliferative response was not altered (not shown).

The effect of CSF CGRP treatment on the morphology of microglia cells was analyzed in Iba1/DAPI stained sections. Microglia morphology could vary dramatically within single fields of both CGRP-treated and control mice (representative examples are reported in Suppl. Fig. 2): the morphology could range from ramified-bipolar (the typical shape in the white matter) to an almost circular-fitting shape, showing a full array of intermediate steps. Since a higher proportion of circular-fitting cells could be noticed, the morphology was quantitatively analyzed by an automatic procedure: this was developed within ImageJ program by creating a home-made macro that used built-in commands. Iba-1-positive objects that were i) associated to DAPI staining, ii) larger than 2000 pixel (50 μm^2) (to discard cell debris), and iii) away from image edges, were selected (see Fig. 3A–D for the result of the analysis of the images in Suppl. Fig. 2). In the Max Intensity Z-projection, single objects that resulted from two cells belonging to different focal planes were manually excluded from analysis (see, e.g., Fig. 3D): percentage of eliminated objects was 5.69% (+/−4.66) in CGRP-treated mice and 10.95% (+/−9.37) in control mice (not significantly different: p = 0.0856; t test). The quantitative morphological analysis was conducted to obtain size- (area, perimeter), shape- (best fit ellipse axes, Feret diameters) and intensity-related (mean) measures. As a reference, the same analysis was conducted in naive and relapsing mice to obtain round values of ramified and bushy microglia, respectively. In order to reach a high proportion of bushy microgliain the images from relapsing mice, the scans were taken from concentric 100 μm thick rings around lesion sites (i.e., sites showing high

density of CD3+ cells: the lesion areas were excluded). The mean round values (the ratio between minor and major axes of cell best fit ellipse) were 0.32 (+/−0.04) (mean+/− st. dev.) and 0.52 (+/−0.04) in naive and relapsing mice, respectively (Fig. 3F) (the difference was statistically significant: p = 0.0032; Student's t test). A round value of 1 indicates an object whose best elliptic-type fit is a circle. An example of a bipolar and a bushy microglia (within the same white matter field of a remitting mouse) is reported in Fig. 3G: their round values were 0.30 and 0.55, respectively. In CGRP-treated and control mice (of CSF spinal delivery experiments) the analysis showed that round value was 0.46 (+/−0.02) in control mice and 0.41 (+/−0.02) in CGRP-treated mice: the difference was statistically significant (p = 0.0056; Student's t test) (Fig. 3E). The result of the analysis did not change when the size of Iba1 objects was decreased (to 1000 pixel) or the threshold level was increased (from 17/255 to 19/255) (not shown). The cell density and all other parameters (area, perimeter, major and minor axes of best fit ellipse, Feret diameters and mean) did not show any significant difference (not shown).

The effect of CGRP treatment on astrocyte reactivity was monitored by analyzing the expression of GFAP, which is modulated during EAE progression: GFAP fluorescence intensity was not significantly different in CGRP-treated and control mice (p = 0.5272; t test) (Suppl. Fig. 3A). Finally, an analysis of EAE-induced infiltration in CNS was carried out in hematoxylin/eosin stained sections: no significant difference in meningeal cell density was found (p = 0.8000; Wilcoxon rank-sum test) (Suppl. Fig. 3B). Similarly, no significant difference was detected in parenchyma infiltrates (not shown).

Since RCP expression is known to correlate with receptor activation and increased CGRP efficacy, we investigated the possible correlation between RCP expression and EAE progression. We first analyzed RCP expression in the spinal cord white matter of naive (control) mice by triple labeling (including DAPI) and confocal analysis. RCP showed a diffuse pattern and was mainly present in cell bodies and processes (Fig. 4A). RCP was detected in astrocytes (labeled by anti-GFAP antibodies; Fig. 4C), bipolar microglia (labeled by Tomato Lectin; Fig. 4D), oligodendrocytes (labeled by anti-CNPase antibodies; Fig. 4F) and endothelial cells of parenchymal vessels (labeled by Tomato Lectin; Fig. 4G). The two microglia markers (TL and Iba-1) exhibited a similar staining pattern in both control and relapse mice. No RCP immunoreactivity was detected in NF 200-positive axonal fibers (not shown). In the spinal cord of EAE mice, RCP immunoreactivity showed a similar pattern of immunoreactivity, but for a slight increase (in non-lesion areas) (Fig. 4B), where RCP was located in the same cell types and, in addition, in bushy (activated) (Fig. 4E) and ameboid microglia as well as in infiltrating lymphocytes (Fig. 4H). In spinal cord white matter of control mice RCP was expressed in 22.37% (+/−9.98) microglia cells (total number of Tomato Lectin/DAPI stained cells = 2007 in 212 microscope fields), 55.50% (+/−19.46) astrocytes (total cell no. = 2968; 258 fields), 83.02% (+/−4.23) oligodendrocytes (total cell no. = 366; 47 fields) and 13.31% (+/−7.66) endothelial cells (total cell no. = 98; 104 fields). RCP was also frequently detected in neuronal cell bodies, including motoneurons, of the spinal cord gray matter (not shown).

In the spinal cord white matter of EAE mice RCP expression was found to be increased, in particular in lesion areas (defined as MBP-negative, CD3-positive areas) (Fig. 5A–D). RCP

expression in CD3+ cells was analyzed in 57 microscope fields from relapsing mice: RCP was expressed in 24.03% (+/−3.53) of parenchymal CD3+ cells (100/424) and 24.56% (+/−11.82) of (peri) vascular CD3 + cells (21/77). A densitometric analysis was conducted by scanning regularly spaced areas in the ventro-medial region of funiculus spanning the whole length of the spinal cord of naive, CFA, remitting and relapsing mice. A significant increase of RCP fluorescence intensity was found in relapsing ($p = 0.0002$; ANOVA-one-way), but not in remitting mice in comparison to controls (Fig. 5E). A regression analysis conducted in relapsing and remitting mice showed absence of correlation with the density of CD3+ cells ($r = 0.0029$ and $r = 0.0024$, respectively) (Fig. 5F, G), indicating that most of RCP fluorescence intensity increase was likely to occur in resident (non-infiltrated) cells. In randomly sampled fields, the total number of RCP+/DAPI+ cells/field in relapsing mice was slightly, but not significantly increased: 2.66 +/−0.81 (mean +/− st. dev.) (median = 2.48) in control mice, 3.23 +/−1.22 (median = 3.90) in relapsing mice ($p = 0.70$; Wilcoxon rank-sum test) (Fig. 5H). RCP expression showed a cell-specific trend in relapsing mice: an increase in RCP+ microglia density (from 0.24 +/−0.11 in control mice to 0.84 +/− 0.17) while a decrease in RCP+ astrocytes (from 1.14 +/− 0.15 to 0.63 +/− 0.38) as well as oligodendrocytes (from 2.48 +/− 0.89 to 1.02 +/− 0.75; see Fig. 5H). However, since the cell-specific markers used to identify the cell types are increased in EAE, statistical analysis could not be performed to evaluate significant cell-specific differences in RCP expression.

Since a putative nuclear localization of RCP signal could be inferred in naive and relapsing mice white matter cells (see, e.g., Fig. 4A, B, D), intracellular RCP localization was further analyzed in vitro and in tissue (following DAPI staining). In vitro, a fibroblast-derived cell line (NIH3T3, endogenously expressing CGRP receptors) showed mainly a membrane fraction localization of RCP, in resting condition: however, following CGRP application RCP showed translocation to the nuclear fraction (Fig. 6A). Nuclear localization was also observed in Venus-RCP-transfected primary microglia. We also attempted a determination of changes in Venus-RCP localization upon CGRPexposure (by automated high throughput microscopy). However, CGRP stimulation did not result in detectable changes in Venus-RCP nuclear distribution, possibly due to the high level of nuclear localization at the resting state (not shown). In CNS tissue from control mice, glia cells exhibited significantly different RCP intracellular localization: RCP nuclear localization was detected in 57.62% (+/−20.98) of RCP+ microglia, 97.23% (+/−3.04) of astrocytes and 100,00% (+/−0.00) of oligodendrocytes (see Fig. 6B, D, F for images, Fig. 6I for histogram). Interestingly, in relapsing mice RCP intracellular localization was altered in a cell-specific manner: nuclear localization significantly increased to 85.03% (+/−10.59; $p = 0.0286$; Wilcoxon rank-sum test) in microglia, but decreased to 74.27% (+/−13.42; $p = 0.0286$; Wilcoxon rank-sum test) in astrocytes; no significant changes were observed in oligodendrocytes (72.51% +/−28.63; $p = 0.1213$; Wilcoxon rank-sum test) (see Fig. 6C, E for images, Fig. 6I for histogram). In aCSF-treated (control) C-EAE mice, RCP nuclear localization was present in 73.73% (+/−7.02) of microglia cells: following CGRP CSF delivery, it increased significantly up to 88.08% (+/−4.97) ($p = 0.0445$; Student's t test) (Fig. 6G). CLR, instead, showed a very low (unchanged) level of nuclear localization, both in control and relapse mice (R-EAE) (10.36% (+/−6.49) and 6.14% (+/−3.50), respectively; $p = 0.3771$, Student's t test) (Fig. 6H).

The changes of RCP expression during disease progression were paralleled by changes of CGRP and adrenomedullin expression in relapsing–remitting EAE mice. In spinal cord of control mice CGRP immunoreactivity was detectable in motoneuron cell bodies of gray matter ventral horns (Fig. 7A–B) and in terminals and fibers of laminae I–II in dorsal horns, whereas adrenomedullin was detectable in terminals and fibers in dorsal horn laminae I–II: no changes in distribution between control and EAE mice were detected (not shown). A densitometric analysis revealed that motoneuron cell bodies express significantly higher levels of CGRP immunoreactivity in relapsing than in control mice (Fig. 7C; $p = 0.0018$; t test). Terminals and fibers of dorsal horn laminae I–II (originating from dorsal root ganglia sensory neurons) showed slight, but not significant differences in CGRP (Fig. 7D; $p = 0.2128$: t test) as well as adrenomedullin immunoreactivity (Fig. 7E; $p = 0.2360$; t test).

4. Discussion

Our results show that the lack of CGRP aggravates EAE signs; moreover, the clinical score recorded in animals that possess different amounts of CGRP alleles showed a “gene-dosage” effect. At the end of the observation period (50 dpi) the neuropathological analysis revealed no immune cell infiltration or demyelinization in either CGRP-null mouse or wild type mouse. However, the 129 strain is known to exhibit a very mild disease when immunized by the present protocol. The site where CGRP exerts its protective activity (within CNS or in the periphery) cannot be ascertained by the present approach.

Very recently, Matsuda et al. (2012) showed that i.v. injection of dendritic cells transfected with CGRP reduced EAE development. During revision of the paper, Pedreño and collaborators reported a similar effect for adrenomedullin (a strongly related peptide that can directly activate the CGRP receptor) (Pedreño et al., 2014). These results support the concept that CGRP and its related peptides can exert a protective role (in the periphery) during EAE pathogenesis. On the other hand, Mikami et al. (2012) showed that RAMP1-deficient mice were resistant to EAE. However, RAMP1 can form complexes with calcitonin receptor (in addition to CLR) to give amylin receptor (referred to as AMY1 receptor; Poyner et al., 2002; Hay et al., 2005) as well as with other family B G protein coupled receptors (such as vasoactive intestinal polypeptide/ pituitary adenylate cyclase activating peptide receptor; Christopoulos et al., 2003). Thus, the RAMP1 knockdown mouse may not be a proper model for studying the effects of CGRP.

In the second experimental model, CGRP was delivered into the CSF by osmotic minipumps. The impact of surgery and the possible leakage of the peptide from CNS were evaluated. The surgery, performed at the level of lumbar spinal cord (the main target of EAE score motor tests), affected the tests only weakly, as the scores of sham-operated mice were low, corresponding to a tail and mild hind limb impairment (gait problems). The leakage has to be considered negligible as the present findings on peripheral lymphocytes failed to reveal any modulation of immune cell function, while it is well known that CGRP is able to profoundly influence lymphocyte release of cytokines (Kawamura et al., 1998; Levite, 1998; Tokoyoda et al., 2004).

The delivery and confinement of CGRP within CNS was sufficient to reduce EAE signs during the initial phase, and, in parallel, to inhibit microglia morphological activation. Since in vitro CGRP inhibits both inflammatory cytokine and NO release from activated microglia, it is likely that the reduction of EAE signs by CGRP delivery into CSF is mediated, at least in part, by inhibition of microglia activation. The involvement of microglia during the initial phase of EAE has already been suggested, but this is the first time in which a direct stimulation of microglia by a neuropeptide interferes with EAE development.

It is noteworthy that some interesting papers recently reported a modulatory role for other (neuro) peptides in EAE, such as neuropeptide Y (Bedoui et al., 2003), vasoactive intestinal peptide (Gonzalez-Rey et al., 2006), pituitary adenylyl cyclase-activating polypeptide (Tan et al., 2009), galanin (Wraith et al., 2009) and opioid growth factor ([Met(5)]-enkephalin; Zagon et al., 2010). Thus, accumulating evidence suggests that (neuro) peptides can be considered as a new class of compounds playing a significant role in neuroinflammation.

The microglia activation has been described in morphological (from ramified to bushy or ameboid shape) or functional terms (from resting to activated to phagocytic activity), accompanied by changes in expression of specific markers, largely in a qualitative rather than in a quantitative manner. Our automatic image analysis procedure took advantage of the change in morphology of white matter microglia cells in pathologic conditions. In ramified (resting) condition, white matter microglia assumes a bipolar shape (see also Gehrmann and Kreutzberg, 1995), whereas the bushy (activated) form had a circular shape. A quantitative measure of the different shape was provided by the present analysis of the round value of ramified/bipolar microglia in control mice vs bushy microglia. While representative examples of the two shapes (from naive and relapsing mice) provided a very large, significant difference in round value, in the CSF CGRP delivery samples microglia assumed a large variety of intermediate shapes. Nonetheless, the mean round value of CGRP-treated mice was significantly smaller and closer to the ramified/bipolar shape than those of control (untreated EAE) mice. The method was not very sensitive to changes in either threshold or object size that was used to eliminate background or cell debris, respectively. The lack of difference in mean area and perimeter of microglia in CGRP-treated and control mice suggests that cells in ramified state in vivo change morphology via process rearrangement.

EAE altered the expression o both peptide and receptor components of the CGRP/adrenomedullin family of peptides. The increase in CGRP expression is in line with the results of Giardino et al. (2004), who, in a different model (spinal cord tissue-induced EAE in Lewis rats), found a transient increase in CGRP mRNA in motoneurons at the disease peak. This increase appears to be restricted to cells resident in spinal cord parenchyma, as no expression changes occur in dorsal horn fibers, that originate from dorsal root ganglion neurons (a finding in accordance with the report by Olechowski et al., 2009).

Even though adrenomedullin and CGRP expression did not change in dorsal horn fibers during EAE pathogenesis, cerebral endothelial cells can secrete a substantial amount of adrenomedullin from their abluminal (brain) side, although the peptide is not detectable by

immunoreactivity (Kis et al., 2002). Moreover, they constitute the major source of circulating adrenomedullin (Kis et al., 2002): thus, blood could be an additional source of CGRP and adrenomedullin during EAE, as local disruption of blood–brain-barrier occurs during disease progression (see Alvarez et al., 2011, for a recent review). Therefore, CGRP and adrenomedullin are likely to be increased in CNS parenchyma during EAE, with sources being CNS cells and/or blood.

RCP expression correlates with receptor activation in uterus and vasculature and its increase results in increased CGRP efficacy (Naghashpour et al., 1997; Supowit et al., 2011). The role of RCP expression as positive indicator of CGRP efficacy and the present evidences of CGRP protective effects in EAE led us to investigate whether a correlation with RCP expression could be present during EAE progression. RCP expression in the spinal cord white matter paralleled the EAE severity and was significantly increased in lesion sites of relapsing mice. The absence of correlation with cell density suggests that the main source of RCP increase should be resident parenchymal cells. It can be suggested that the overall increase in RCP expression in EAE should be attributed mostly to expression increase in individual cells. Similar to our findings, RCP expression in dorsal horn of spinal cord has been observed to increase in response to administration of CGRP antagonist and in response to carrageenan-induced or sciatic nerve ligation-induced inflammation (Ma et al., 2003). Thus, activation of the CGRP/adrenomedullin receptor system appears to be a general response to inflammation in the spinal cord.

A previous study described RCP immunostaining in the nucleus of motoneurons and cerebellar Purkinje cells (Ma et al., 2003). However, our findings are the first to describe the dynamic movement of RCP between cytoplasm and nucleus, in cell cultures in response to ligand, and in vivo in microglia in response both to a pathological condition and to exogenous CGRP application. The nuclear localization of RCP suggests a potential transcriptional role for RCP. In support to this hypothesis, the yeast orthologue of RCP was described as a subunit for yeast RNA polymerase III (Siaut et al., 2003). Accordingly, RCP translocation to the nucleus suggests an additional signaling pathway for the CGRP receptor in mammalian cells. In this context, it can be hypothesized that altered RCP nuclear localization in glia cells might represent a novel mechanism by which CGRP influences EAE pathogenesis. Interestingly, specific glia cells show differential levels of RCP trafficking, which suggests cell-specific responses to CGRP. The response does not seem to involve a membrane component (CLR) of the receptor. Based on results from other G protein-coupled receptors (Goetzl, 2007) the nuclear translocation of receptor membrane components could be hypothesized. However, the present findings show a very limited level of CLR nuclear localization in both control and relapse mice. It has to be mentioned that CLR nuclear localization was found absent in the trigeminal ganglion (Eftekhari et al., 2010). The novel mechanism mediating CGRP response seems thus to concern only the cytoplasmic component of the receptor. This was not unexpected as a differential intracellular regulation of CLR and RAMP1 (following CGRP stimulation) has already been described (Cottrell et al., 2007).

The present findings, together with our previous investigation on the CGRP/adrenomedullin anti-inflammatory inhibition of microglia activation in vitro (Consonni et al., 2011) allow us

to suggest that these peptides can act as CNS homeostatic factors that counterbalance ongoing deleterious inflammation in EAE, by targeting CNS cells. Microglia activation is being considered as one of the crucial factors of EAE pathogenesis (Heppner et al., 2005; Ponomarev et al., 2006; Gao and Tsirka, 2011; Ramaglia et al., 2012) and its inhibition by CGRP is likely to mediate the peptide protective effect. Moreover, such an effect possibly involves a novel pathway, the cell-specific nuclear translocation of the receptor or at least of a cytoplasmic component of it, RCP.

Supplementary Material

Refer to Web version on PubMed Central for supplementary material.

Acknowledgments

Part of this work was carried out in Alembic, the Advanced Light and Electron Microscopy Bio-Imaging Centre of San Raffaele Scientific Institute and within the framework of the Ivascomar project, Cluster Tecnologico Nazionale Scienze della Vita ALISEI (Italian Ministry of Research).

Funding statement: Financial support were from FISM - Fondazione Italiana Sclerosi Multipla (www.aism.it) cod. 2011/R/27 (SM), NUTEC - Regione Lombardia 2013–2014, Biotecnology: ID 30263049 (SM), PNR-CNR Aging Program 2012–2014 (www.cnr.it) (SM), the Italian Ministry of Research - PRIN (prin.miur.it) (proj. 2006054051: FG), the Comitato Telethon Fondazione Onlus (www.telethon.it) (GGP10099 grant: FG) and the NIH (www.nih.gov) grant no. DK52328 (IMD).

References

Alvarez JI, Cayrol R, Prat A. Disruption of central nervous system barriers in multiple sclerosis. Biochim Biophys Acta. 2011; 1812:252–264. [PubMed: 20619340]

Amara SG, Jonas V, Rosenfeld MG, Ong ES, Evans RM. Alternative RNA processing in calcitonin gene expression generates mRNAs encoding different polypeptide products. Nature. 1982; 298:240–244. [PubMed: 6283379]

Ashizuka S, Ishikawa N, Kato J, Yamaga J, Inatsu H, Eto T, Kitamura K. Effect of adrenomedullin administration on acetic acid-induced colitis in rats. Peptides. 2005; 26:2610–2615. [PubMed: 15978699]

Baker D, Amor S. Publication guidelines for refereeing and reporting on animal use in experimental autoimmune encephalomyelitis. J Neuroimmunol. 2012; 242:78–83. [PubMed: 22119102]

Bedoui S, Miyake S, Lin Y, Miyamoto K, Oki S, Kawamura N, Beck-Sickinger A, von Hörsten S, Yamamura T. Neuropeptide Y (NPY) suppresses experimental autoimmune encephalomyelitis: NPY1 receptor-specific inhibition of autoreactive Th1 responses in vivo. J Immunol. 2003; 171:3451–3458. [PubMed: 14500640]

Carrizo GJ, Wu R, Cui X, Dwivedi AJ, Simms HH, Wang P. Adrenomedullin and adrenomedullin-binding protein-1 downregulate inflammatory cytokines and attenuate tissue injury after gut ischemia–reperfusion. Surgery. 2007; 141:245–253. [PubMed: 17263982]

Chang CL, Roh J, Hsu SY. Intermedin, a novel calcitonin family peptide that exists in teleosts as well as in mammals: a comparison with other calcitonin/intermedin family peptides in vertebrates. Peptides. 2004; 25:1633–1642. [PubMed: 15476930]

Christopoulos A, Christopoulos G, Morfis M, Udawela M, Laburthe M, Couvineau A, Kuwasako K, Tilakaratne N, Sexton PM. Novel receptor partners and function of receptor activity-modifying proteins. J Biol Chem. 2003; 278:3293–3297. [PubMed: 12446722]

Clementi G, Floriddia ML, Prato A, Marino A, Drago F. Adrenomedullin and ocular inflammation in the rabbit. Eur J Pharmacol. 2000; 400:321–326. [PubMed: 10988350]

Consonni A, Morara S, Codazzi F, Grohovaz F, Zacchetti D. Inhibition of lipopolysaccharide-induced microglia activation by calcitonin gene related peptide and adrenomedullin. Mol Cell Neurosci. 2011; 48:151–160. [PubMed: 21803157]

Cottrell GS, Padilla B, Pikios S, Roosterman D, Steinhoff M, Grady EF, Bunnett NW. Post-endocytic sorting of calcitonin receptor-like receptor and receptor activity-modifying protein 1. J Biol Chem. 2007; 282:12260–12271. [PubMed: 17310067]

Cui X, Wu R, Zhou M, Dong W, Ulloa L, Yang H, Wang H, Tracey KJ, Simms HH, Wang P. Adrenomedullin and its binding protein attenuate the proinflamma-tory response after hemorrhage. Crit Care Med. 2005; 33:391–398. [PubMed: 15699844]

Dackor R, Caron K. Mice heterozygous for adrenomedullin exhibit a more extreme inflammatory response to endotoxin-induced septic shock. Peptides. 2007; 28:2164–2170. [PubMed: 17889965]

D'Antoni S, Zambusi L, Codazzi F, Zacchetti D, Grohovaz F, Provini L, Catania MV, Morara S. Calcitonin gene-related peptide (CGRP) stimulates Purkinje cell dendrite growth in culture. Neurochem Res. 2010; 35:2135–2143. [PubMed: 20960054]

Ding W, Stohl LL, Wagner JA, Granstein RD. Calcitonin gene-related peptide biases Langerhans cells toward Th2-type immunity. J Immunol. 2008; 181:6020–6026. [PubMed: 18941191]

Durham PL. Calcitonin gene-related peptide (CGRP) and migraine. Headache. 2006; 46(Suppl. 1):S3–S8. [PubMed: 16927957]

Eftekhari S, Salvatore CA, Calamari A, Kane SA, Tajti J, Edvinsson L. Differential distribution of calcitonin gene-related peptide and its receptor components in the human trigeminal ganglion. Neuroscience. 2010; 25:683–696. [PubMed: 20472035]

Egea SC, Dickerson IM. Direct interactions between calcitonin-like receptor (CLR) and CGRP-receptor component protein (RCP) regulate CGRP receptor signaling. Endocrinology. 2012; 153:1850–1860. [PubMed: 22315449]

Engelhardt B, Ransohoff RM. The ins and outs of T-lymphocyte trafficking to the CNS: anatomical sites and molecular mechanisms. Trends Immunol. 2005; 26:485–495. [PubMed: 16039904]

Evans BN, Rosenblatt MI, Mnayer LO, Oliver KR, Dickerson IM. CGRP-RCP, a novel protein required for signal transduction at calcitonin gene-related peptide and adrenomedullin receptors. Biol Chem. 2000; 275:31438–31443.

Fernandez S, Knopf MA, McGillis JP. Calcitonin-gene related peptide (CGRP) inhibits interleukin-7-induced pre-B cell colony formation. J Leukoc Biol. 2000; 67:669–676. [PubMed: 10811007]

Flugel A, Bradl M, Kreutzberg GW, Graeber MB. Transformation of donor-derived bone marrow precursors into host microglia during autoimmune CNS inflammation and during the retrograde response to axotomy. J Neurosci Res. 2001; 66:74–82. [PubMed: 11599003]

Furlan R, Cuomo C, Martino G. Animal models of multiple sclerosis. Methods Mol Biol. 2009; 549:157–173. [PubMed: 19378202]

Gao, Z.; Tsirka, SE. Animal models of MS reveal multiple roles of microglia in disease pathogenesis. Neurol Res Int. 2011. http://dx.doi.org/10.1155/2011/383087 (Article ID 383087)

Gehrmann, J.; Kreutzberg, GW. Microglia in experimental neuropathology. In: Kettenmann, H.; Ransom, BA., editors. Neuroglia. Oxford University Press; New York: 1995. p. 883-904.

Giardino L, Giuliani A, Fernandez M, Calzà L. Spinal motoneurone distress during experimental allergic encephalomyelitis. Neuropathol Appl Neurobiol. 2004; 30:522–531. [PubMed: 15488028]

Goetzl EJ. Diverse pathways for nuclear signaling by G protein-coupled receptors and their ligands. FASEB J. 2007; 21:638–42. [PubMed: 17194692]

Gomes RN, Castro-Faria-Neto HC, Bozza PT, Soares MB, Shoemaker CB, David JR, Bozza MT. Calcitonin gene-related peptide inhibits local acute inflammation and protects mice against lethal endotoxemia. Shock. 2005; 24:590–594. [PubMed: 16317392]

Gonzalez-Rey E, Fernandez-Martin A, Chorny A, Martin J, Pozo D, Ganea D, Delgado M. Therapeutic effect of vasoactive intestinal peptide on experimental autoimmune encephalomyelitis. Down-regulation of inflammatory and autoimmune responses. Am J Pathol. 2006; 168:1179–1188. [PubMed: 16565493]

Gonzalez-Rey E, Chorny A, O'Valle F, Delgado M. Adrenomedullin protects from experimental arthritis by down-regulating inflammation and Th1 response and inducing regulatory T cells. Am J Pathol. 2007; 170:263–271. [PubMed: 17200199]

Hay DL, Christopoulos G, Christopoulos A, Poyner DR, Sexton PM. Pharmacological discrimination of calcitonin receptor: receptor activity-modifying protein complexes. Mol Pharmacol. 2005; 67:655–1665. [PubMed: 15576634]

Heppner FL, Greter M, Marino D, Falsig J, Raivich G, Hövelmeyer N, Waisman A, Rülicke T, Prinz M, Priller J, Becher B, Aguzzi A. Experimental autoimmune encephalomyelitis repressed by microglial paralysis. Nat Med. 2005; 11:146–152. [PubMed: 15665833]

Holzer P. Neurogenic vasodilatation and plasma leakage in the skin. Gen Pharmacol. 1998; 30:5–11. [PubMed: 9457475]

Kawamura N, Tamura H, Obana S, Wenner M, Ishikawa T, Nakata A, Yamamoto H. Differential effects of neuropeptides on cytokine production by mouse helper T cell subsets. Neuroimmunomodulation. 1998; 5:9–15. [PubMed: 9698253]

Kis B, Kaiya H, Nishi R, Deli MA, Abraham CS, Yanagita T, Isse T, Gotoh S, Kobayashi H, Wada A, Niwa M, Kangawa K, Greenwood J, Yamashita H, Ueta Y. Cerebral endothelial cells are a major source of adrenomedullin. J Neuroendocrinol. 2002; 14:283–293. [PubMed: 11963825]

Kitamura K, Kangawa K, Kawamoto M, Ichiki Y, Nakamura S, Matsuo H, Eto T. Adrenomedullin: a novel hypotensive peptide isolated from human pheochromocy-toma. Biochem Biophys Res Commun. 1993; 192:553–560. [PubMed: 8387282]

Kroeger I, Erhardt A, Abt D, Fischer M, Biburger M, Rau T, Neuhuber WL, Tiegs G. The neuropeptide calcitonin gene-related peptide (CGRP) prevents inflammatory liver injury in mice. J Hepatol. 2009; 51:342–353. [PubMed: 19464067]

Levite M. Neuropeptides, by direct interaction with T cells, induce cytokine secretion and break the commitment to a distinct T helper phenotype. Proc Natl Acad Sci U S A. 1998; 95:12544–12549. [PubMed: 9770522]

Lu JT, Son YJ, Lee J, Jetton TL, Shiota M, Moscoso L, Niswender KD, Loewy AD, Magnuson MA, Sanes JR, Emeson RB. Mice lacking alpha-calcitonin gene-related peptide exhibit normal cardiovascular regulation and neuromuscular development. Mol Cell Neurosci. 1999; 14:99–120. [PubMed: 10532808]

Lucchinetti C, Bruck W, Parisi J, Scheithauer B, Rodriguez M, Lassmann H. Heterogeneity of multiple sclerosis lesions: implications for the pathogenesis of demyelination. Ann Neurol. 2000; 47:707–717. [PubMed: 10852536]

Ma W, Chabot JG, Powell KJ, Jhamandas K, Dickerson IM, Quirion R. Localization and modulation of calcitonin gene-related peptide-receptor component protein-immunoreactive cells in the rat central and peripheral nervous systems. Neuroscience. 2003; 120:677–694. [PubMed: 12895509]

Ma W, Chabot JG, Quirion R. A role for adrenomedullin as a pain-related peptide in the rat. Proc Natl Acad Sci U S A. 2006; 103:16027–16032. [PubMed: 17043245]

Matsuda R, Kezuka T, Nishiyama C, Usui Y, Matsunaga Y, Okunuki Y, Yamakawa N, Ogawa H, Okumura K, Goto H. Suppression of murine experimental autoimmune optic neuritis by mature dendritic cells transfected with calcitonin gene-related peptide gene. Invest Ophthalmol Vis Sci. 2012; 53:5475–5485. [PubMed: 22807299]

McGillis JP, Humphreys S, Rangnekar V, Ciallella J. Modulation of B lymphocyte differentiation by calcitonin gene-related peptide (CGRP). II. Inhibition of LPS-induced kappa light chain expression by CGRP. Cell Immunol. 1993; 150:405–416. [PubMed: 8396499]

McLatchie LM, Fraser NJ, Main MJ, Wise A, Brown J, Thompson N, Solari R, Lee MG, Foord SM. RAMPs regulate the transport and ligand specificity of the calcitonin-receptor-like receptor. Nature. 1998; 393:333–339. [PubMed: 9620797]

Mikami N, Watanabe K, Hashimoto N, Miyagi Y, Sueda K, Fukada S, Yamamoto H, Tsujikawa K. Calcitonin gene-related peptide enhances experimental autoimmune encephalomyelitis by promoting Th17 cell functions. Int Immunol. 2012; 24:681–691. [PubMed: 22843730]

Morara S, Rosina A, Provini L, Forloni G, Caretti A, Wimalawansa SJ. Calcitonin gene-related peptide receptor expression in the neurons and glia of developing rat cerebellum: an autoradiographic and immunohistochemical analysis. Neuroscience. 2000; 100:381–391. [PubMed: 11008176]

Morara S, Wang LP, Filippov V, Dickerson IM, Grohovaz F, Provini L, Kettenmann H. Calcitonin gene-related peptide (CGRP) triggers Ca^{2+} responses in cultured as-trocytes and in Bergmann glial cells from cerebellar slices. Eur J Neurosci. 2008; 28:2213–2220. [PubMed: 19046367]

Naghashpour M, Rosenblatt MI, Dickerson IM, Dahl GP. Inhibitory effect of calcitonin gene-related peptide on myometrial contractility is diminished at parturition. Endocrinology. 1997; 138:4207–4214. [PubMed: 9322931]

Olechowski CJ, Truong JJ, Kerr BJ. Neuropathic pain behaviours in a chronic-relapsing model of experimental autoimmune encephalomyelitis (EAE). Pain. 2009; 141:156–164. [PubMed: 19084337]

Pedreño M, Morell M, Robledo G, Souza-Moreira L, Forte-Lago I, Caro M, O'Valle F, Ganea D, Gonzalez-Rey E. Adrenomedullin protects from experimental autoimmune encephalomyelitis at multiple levels. Brain Behav Immun. 2014; 37:152–163. [PubMed: 24321213]

Ponomarev ED, Shriver LP, Dittel BN. CD40 expression by microglial cells is required for their completion of a two-step activation process during central nervous system autoimmune inflammation. J Immunol. 2006; 176:1402–1410. [PubMed: 16424167]

Poyner DR, Sexton PM, Marshall I, Smith DM, Quirion R, Born W, Muff R, Fischer JA, Foord SM. International union of pharmacology. XXXII. The mammalian calcitonin gene-related peptides, adrenomedullin, amylin, and calcitonin receptors. Pharmacol Rev. 2002; 54:233–246. [PubMed: 12037140]

Ramaglia V, Hughes TR, Donev RM, Ruseva MM, Wu X, Huitinga I, Baas F, Neal JW, Morgan BP. C3-dependent mechanism of microglial priming relevant to multiple sclerosis. Proc Natl Acad Sci U S A. 2012; 109:965–970. [PubMed: 22219359]

Siaut M, Zaros C, Levivier E, Ferri ML, Court M, Werner M, Callebaut I, Thuriaux P, Sentenac A, Conesa C. An Rpb4/Rpb7-like complex in yeast RNA polymerase III contains the orthologue of mammalian CGRP-RCP. Mol Cell Biol. 2003; 23:195–205. [PubMed: 12482973]

Supowit SC, Katki KA, Hein TW, Gupta P, Kuo L, Dickerson IM, Dipette DJ. Vascular reactivity to calcitonin gene-related peptide is enhanced in subtotal nephrectomy-salt induced hypertension. Am J Physiol Heart Circ Physiol. 2011; 301:H683–H688. [PubMed: 21666123]

Tan YV, Abad C, Lopez R, Dong H, Liu S, Lee A, Gomariz RP, Leceta J, Waschek JA. Pituitary adenylyl cyclase-activating polypeptide is an intrinsic regulator of Treg abundance and protects against experimental autoimmune encephalomyelitis. Proc Natl Acad Sci. 2009; 106:2012–2017. [PubMed: 19190179]

Tokoyoda K, Tsujikawa K, Matsushita H, Ono Y, Hayashi T, Harada Y, Abe R, Kubo M, Yamamoto H. Up-regulation of IL-4 production by the activated cAMP/ cAMP-dependent protein kinase (protein kinase A) pathway in CD3/CD28-stimulated naive T cells. Int Immunol. 2004; 16:643–653. [PubMed: 15096485]

Tsujikawa K, Yayama K, Hayashi T, Matsushita H, Yamaguchi T, Shigeno T, Ogitani Y, Hirayama M, Kato T, Fukada S, Takatori S, Kawasaki H, Okamoto H, Ikawa M, Okabe M, Yamamoto H. Hypertension and dysregulated proinflammatory cytokine production in receptor activity-modifying protein 1-deficient mice. Proc Natl Acad Sci U S A. 2007; 104:16702–16707. [PubMed: 17923674]

Uezono Y, Nakamura E, Ueda Y, Shibuya I, Ueta Y, Yokoo H, Yanagita T, Toyohira Y, Kobayashi H, Yanagihara N, Wada A. Production of cAMP by adrenomedullin in human oligodendroglial cell line KG1C: comparison with calcitonin gene-related peptide and amylin. Brain Res Mol Brain Res. 2001; 97:59–69. [PubMed: 11744163]

Umeda Y, Takamiya M, Yoshizaki H, Arisawa M. Inhibition of mitogen-stimulated T lymphocyte proliferation by calcitonin gene-related peptide. Biochem Biophys Res Commun. 1988; 154:227–235. [PubMed: 2840066]

von der Hardt K, Kandler MA, Popp K, Schoof E, Chada M, Rascher W, Dötsch J. Aerosolized adrenomedullin suppresses pulmonary transforming growth factor-beta1 and interleukin-1 beta gene expression in vivo. Eur J Pharmacol. 2002; 457:71–76. [PubMed: 12460645]

Wang Z, Ma W, Chabot JG, Quirion R. Cell-type specific activation of p38 and ERK mediates calcitonin gene-related peptide involvement in tolerance to morphine-induced analgesia. FASEB J. 2009; 23:2576–2586. [PubMed: 19299480]

Wong LY, Cheung BM, Li YY, Tang F. Adrenomedullin is both proinflammatory and antiinflammatory: its effects on gene expression and secretion of cytokines and macrophage migration inhibitory factor in NR8383 macrophage cell line. Endocrinology. 2005; 146:1321–1327. [PubMed: 15576460]

Wraith DC, Pope R, Butzkueven H, Holder H, Vanderplank P, Lowrey P, Day MJ, Gundlach AL, Kilpatrick TJ, Scolding N, Wynick D. A role for galanin in human and experimental inflammatory demyelination. Proc Natl Acad Sci. 2009; 106:15466–15471. [PubMed: 19717462]

Wu R, Wang P. Preclinical studies with adrenomedullin and its binding protein as cardiovascular protective agents for hemorrhagic shock. Cardiovasc Drug Rev. 2006; 24:204–213. [PubMed: 17214597]

Zagon IS, Rahn KA, Bonneau RH, Turel AP, McLaughlin PJ. Opioid growth factor suppresses expression of experimental autoimmune encephalomyelitis. Brain Res. 2010; 1310:154–161. [PubMed: 19931226]

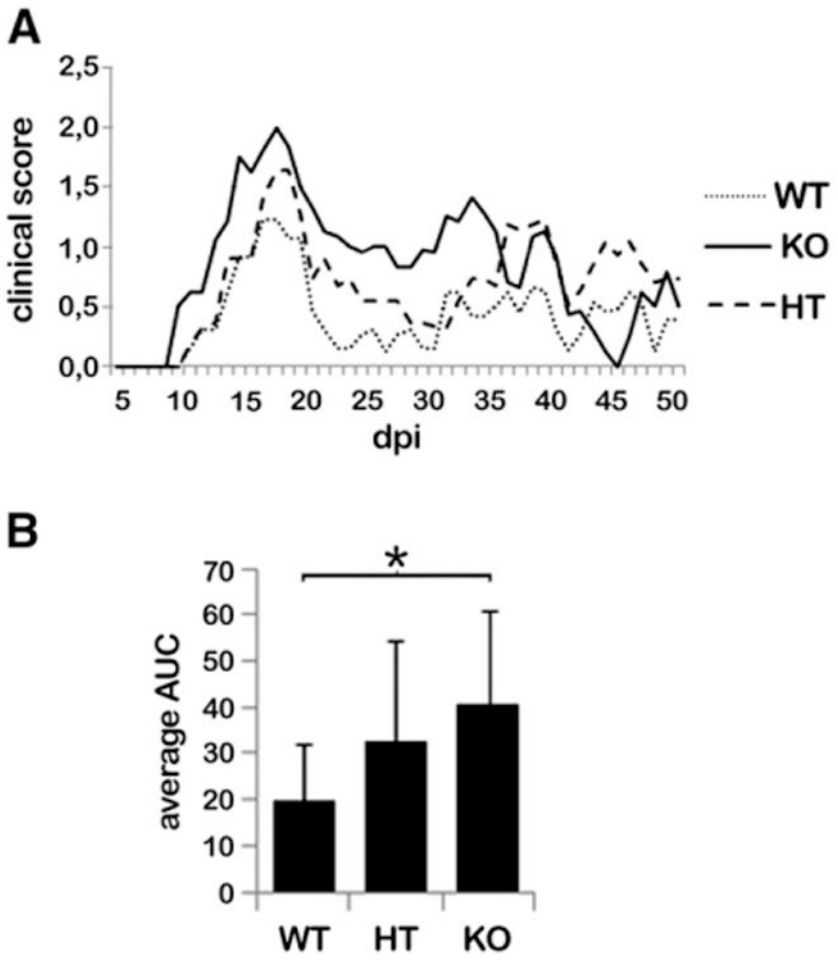

Fig. 1.

Alpha-CGRP gene deficiency aggravated EAE signs. A) The graph depicts the daily average clinical score for wild type (WT), alpha-CGRP null mutant (KO) and heterozygote (HT) mice. B) Cumulative index of the clinical score was significantly increased in alpha-CGRP null mutant mice ($p = 0.0469$; Mann–Whitney U test). Chronic EAE was induced in 129S6 mice ($n = 36$; 13 wild type, WT; 12 alpha-CGRP deficient, KO; 11 heterozygote mice, HT; dpi = day post immunization).

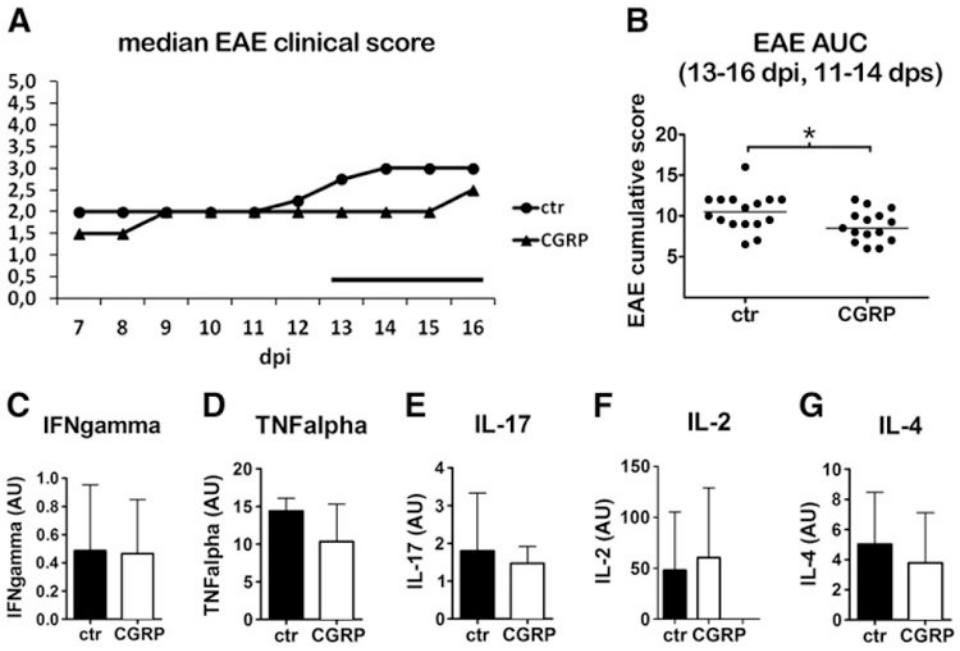

Fig. 2.

Lumbar CSF administration of CGRP decreased clinical score in EAE mice. Two days after EAE immunization (2 days post-immunization, dpi) minipumps were implanted and CGRP (or aCSFascontrol) was delivered for 14 days into lumbar CSF (end of treatment: 16dpi; 16dpi = 14 days post-surgery, dps) (control EAE mice: n = 16, CGRP-treated EAE mice: n=15; chronic EAE in C57BL/6 mice). A) CGRP-treated mice exhibited a delay in EAE onset, compared to control mice. The bar indicates the period (just after EAE onset) that was analyzed for statistics (see Fig. 1B). B) CGRP-treated mice exhibited a significantly lower cumulative score than control EAE mice ($p = 0.037$; Mann–Whitney U test). C–G) Peripheral lymphocytes of CGRP-treated mice did not show any change in the production of IFNgamma (C), TNFalpha (D), IL-17 (E), IL-2 (F) and IL-4 (G) when stimulated with the nominal antigen (MOG). ctr = control; AUC = area under curve. In C-G the mean +/− st. dev. are shown.

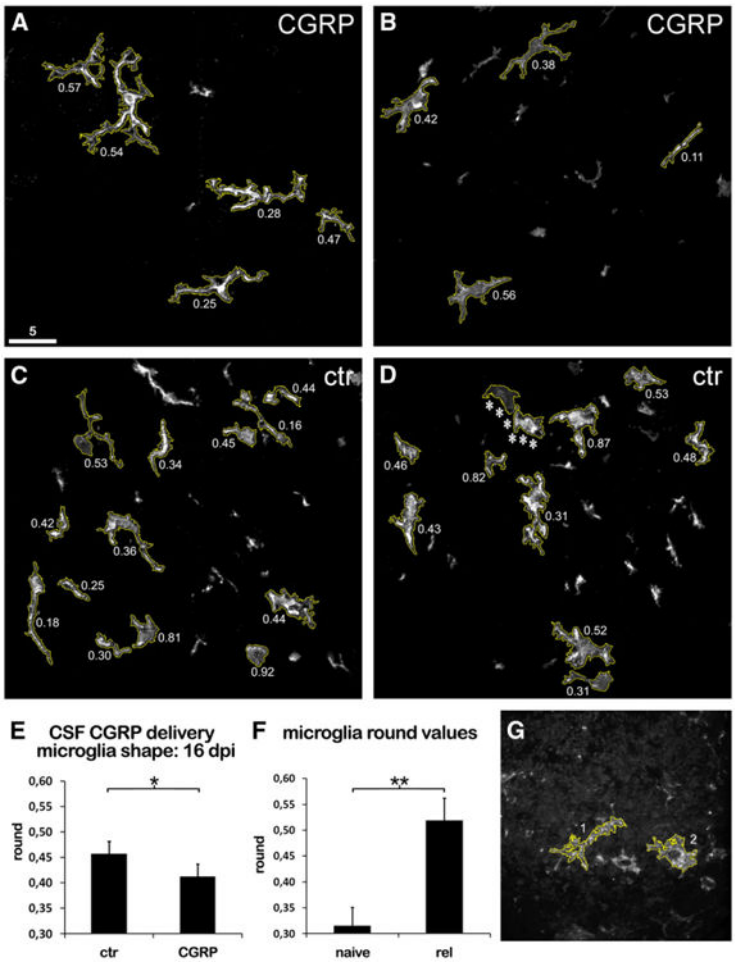

Fig. 3.

Lumbar CSF administration of CGRP reduced microglia transition to bushy morphology. A–D) Iba1+ microglia showed slightly more bipolar and less round-fitting morphology in CGRP-treated (A–B) than control (C–D) mice (representative examples; max intensity projections; chronic EAE in C57BL/6 mice). The cells have been automatically selected by DAPI staining (shown in Suppl. Fig. 3). Yellow boundaries highlight cells automatically selected for analysis: i) size >2000 pixel, ii) not located on edges. Round values (range: 0 to 1) are reported: round = ratio between minor and major axes of best-fit ellipse. Mean round values were 0.40 (+/−0.16) (mean +/− st. dev.) in the CGRP (A–B) images, and 0.47 (+/−0.21) in the ctr (C–D) images. Asterisk row: object manually excluded as originating from two cells located at different focal planes. E) Mean round value in CGRP-treated mice (0.41 +/−0.02) were significantly lower than in ctr mice (0.46 +/−0.02) ($p = 0.0056$; t test). CGRP-treated and control mice: n = 5 mice each; 34–48 scans/mice; 978 and 1315 cells analyzed, respectively. F) Mean round values in normal white matter (in naive mice: 0.32 +/−0.04) were significantly lower than in areas enriched in bushy cells (in relapsing mice: 0.52 +/−0.04) ($p = 0.0032$; t test). The bushy cell-enriched areas were taken from concentric 100 μm thick rings around lesions (i.e., with high density of CD3+ cells) in relapsing mice. Naive and relapsing mice: n = 3 mice each; 18–40 scans/mice; 79 and 101 cells analyzed, respectively. G) Representative examples of microglia cell morphology: bipolar-ramified

(cell 1; round value = 0.30) and bushy (cell 2; round value = 0.55) microglia in a section of a remitting mouse (relapsing–remitting EAE was induced in SJL mice; Tomato Lectin staining). Note the typical bipolar shape of non-reactive microglia in the white matter (cell 1). ctr = control; rel = relapsing; dpi = day post immunization.

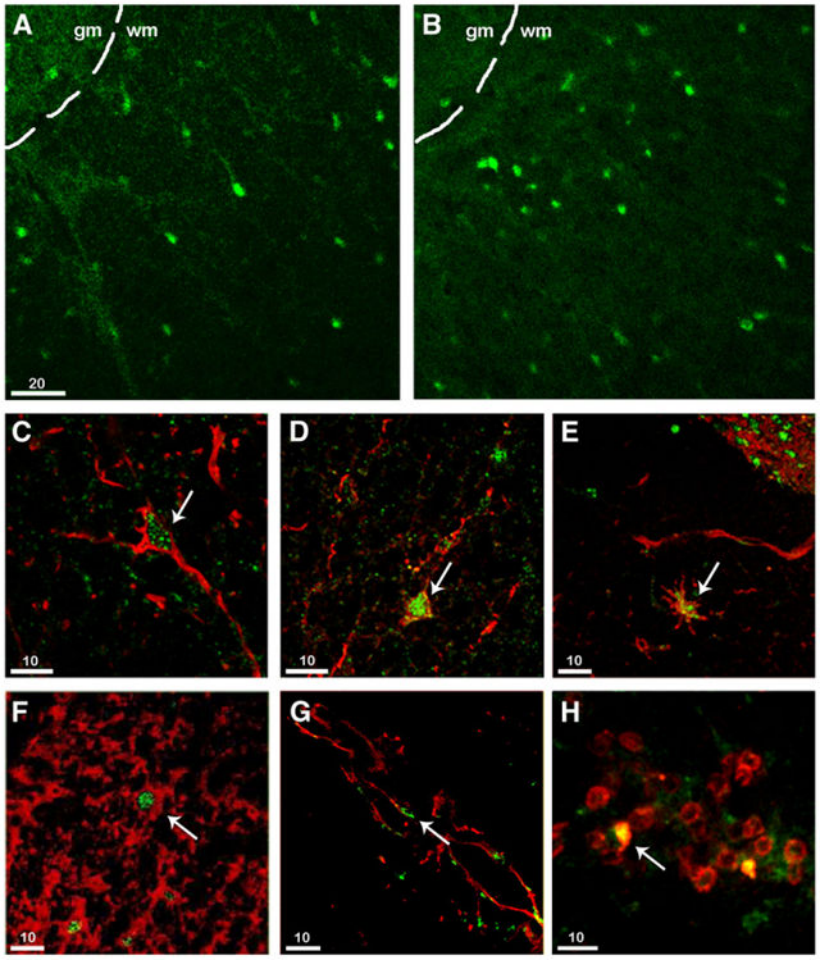

Fig. 4.

RCP immunoreactivity in spinal cord cells of control and EAE mice. RCP (green) was widely expressed in spinal cord cell populations. A similar pattern was detected in both control (A) and relapsing (B) mice: in non-lesion areas of relapsing mice (as in B) a small increase in immunoreactivity could be noticed (B). RCP was localized in GFAP+ astrocytes (C, red), Tomato Lectin+ ramified-bipolar microglia (D, red), Tomato Lectin+ bushy microglia (E, red), CNPase+ oligodendrocytes (F, red), Tomato Lectin+ endothelial cells (G, red), and CD3+ infiltrated lymphocytes (H, red). A, C, D, F = control mice; B, E, H = EAE mice. Calibration bars: 20 μm in A–B, 10 μm in C–H; gm = gray matter; wm = white matter.

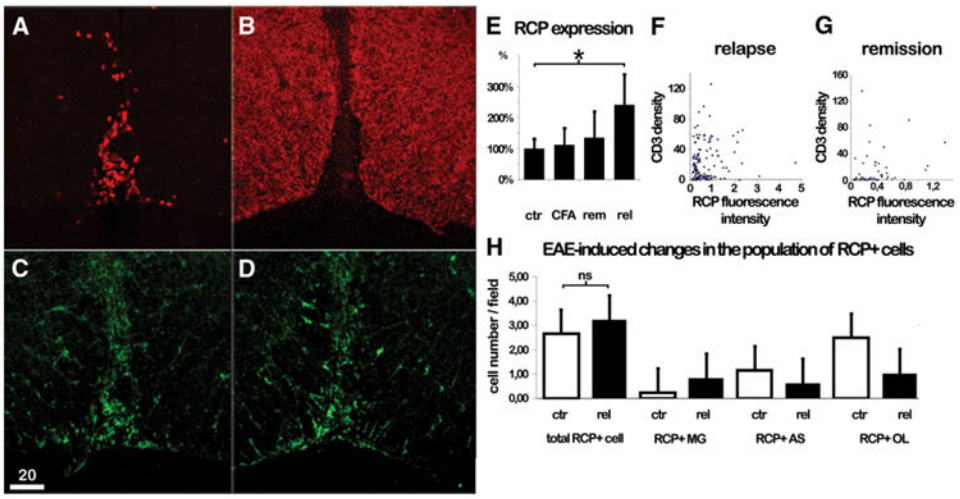

Fig. 5.

RCP immunoreactivity showed an increase in the spinal cord of EAE mice. A–D) In an area of increased CD3+ cell density (A: red) high levels of RCP immunoreactivity (C: green) were detectable. A contiguous section showed MBP-depletion (B: red) in the same area (together with RCP increase; D: green). Calibration bars: 20 μm. E) A densitometric analysis of RCP expression immunofluorescence (expressed as percentage of control (ctr) values) showed a progressive increase along the scale CFA-injected < remitting (rem) < relapsing (rel) mice. In relapsing mice RCP increase was statistically significant ($p = 0.0002$; ANOVA-one-way analysis). 8–9 scans/mice, mice: n = 3 for each group (ctr, CFA, rem, rel). F,G) A regression analysis of RCP immunofluorescence vs CD3+ cell density in the white matter showed absence of correlation: $r = 0.0029$ and $r = 0.0024$ in relapsing and remitting mice, respectively. 2–5 scans/section; 9–12 sections/mouse (a total of 56 and 134 scans were analyzed from remitting and relapsing mice, respectively). H) Total RCP+ cell density did not vary significantly in EAE mice ($p = 0.70$; Wilcoxon rank-sum test), but a trend toward cell-specific changes seemed to occur (increase of RCP+ microglia, MG, density and decrease of RCP+ astrocytes, AS, and oligo-dendrocytes, OL) (not statistically analyzable due to changes in expression of the cell-specific markers). Mice number: n = 4 for each group (ctr, CFA, rem, rel); 16–67 scans/mice. Number of scans (ctr vs relapse, respectively): 212 vs 134 (for microglia), 258 vs 101 (for astrocytes), 47 vs 77 (for oligodendrocytes). ctr = control; CFA = complete Freund's adjuvant; rem = remitting; rel = relapsing

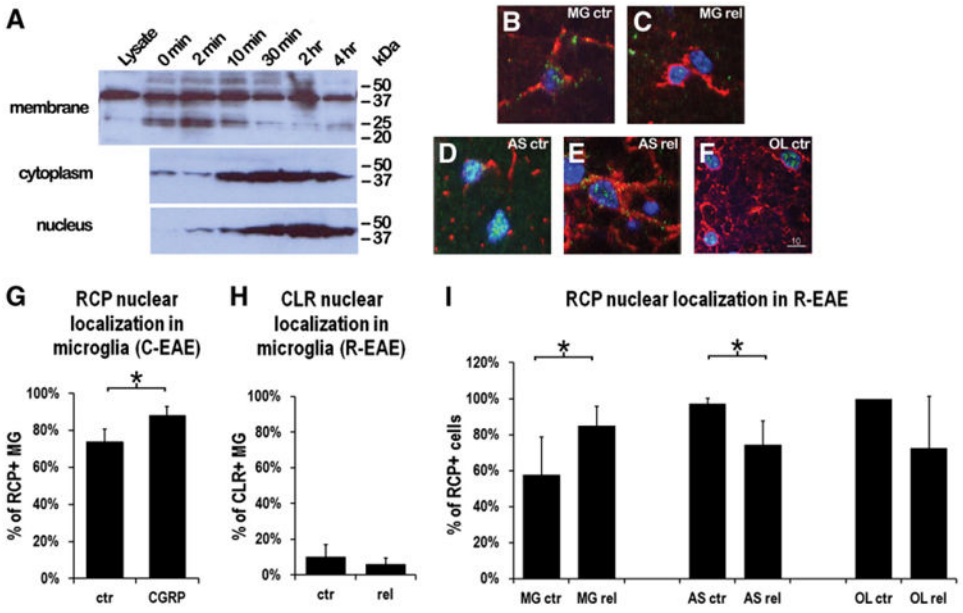

Fig. 6.

RCP intracellular localization was modulated by CGRP and EAE (in a cell-specific manner). A) Changes in RCP intracellular distribution in NIH3T3 cells following CGRP stimulation (representative experiment). Cells were challenged with 100 nM CGRP for the indicated times, homogenized, and membrane, cytoplasmic, and nuclear fractions were separated by centrifugation and analyzed by SDS-PAGE and Western blotting (using antibodies raised against RCP). B–F) RCP intracellular distribution in microglia of control (B) and relapsing mice (C), astrocytes of control mice (D) and relapsing mice (E), and oligodendrocytes of control mice (F). Confocal images, single focal planes. For statistical analysis, see histogram in I. G) RCP nuclear localization significantly increased in RCP+ microglia of C-EAE mice treated with aCSF (ctr) or CGRP CSF delivery ($p = 0.0445$; $n = 3$ for each group; Student's t test). H) CLR nuclear localization was low and unchanged in CLR+ microglia of R-EAE mice. I) RCP nuclear localization in glial cells in control and relapsing mice. Same mice as in B–F. Nuclear localization was significantly increased in microglia (MG) ($p = 0.0286$; Wilcoxon rank-sum test), but decreased in astrocytes (AS) ($p = 0.0286$; Wilcoxon rank-sum test). $n = 4$ for each group (ctr, CFA, rem, rel). MG = microglia; AS = astrocytes; OL = oligodendrocyte; ctr = control; rel = relapsing.

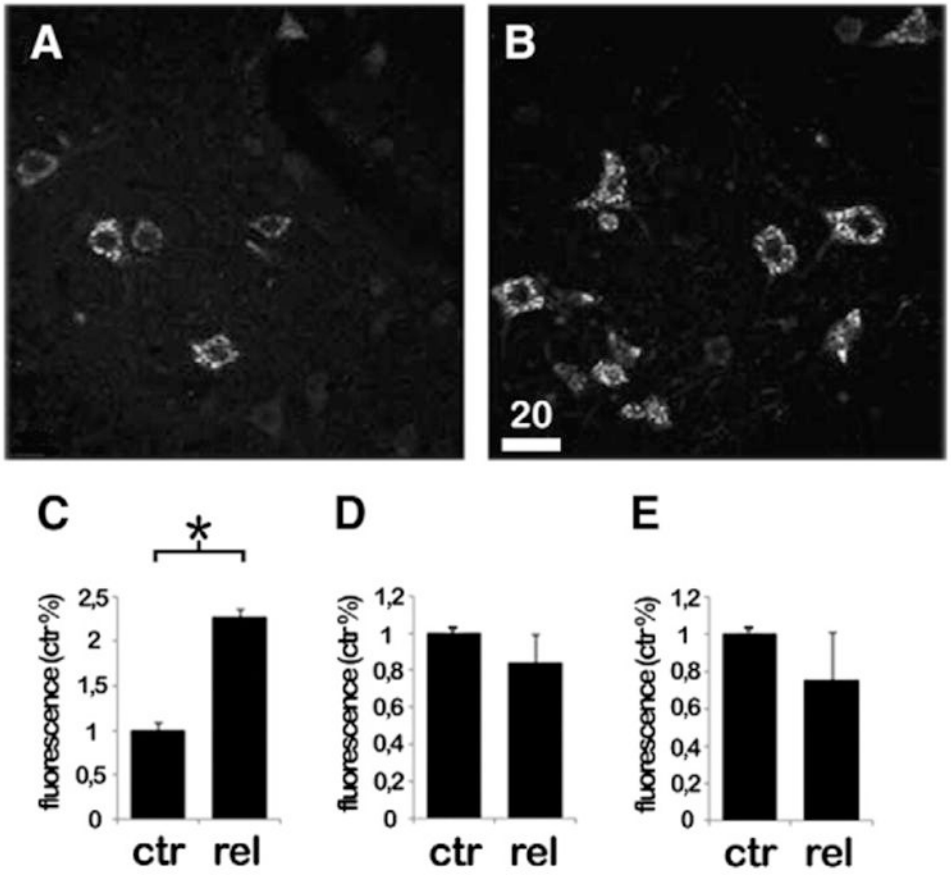

Fig. 7.

CGRP immunoreactivity increased in motoneurons of EAE mice. A, B) Representative examples of CGRP immunoreactivity in motoneurons of a control (A) and relapse (B) lumbar spinal cord sections at corresponding spinal cord levels. Calibration bars: 20μm. C–E) Densitometric analysis of changes in CGRP immunoreactivity in motoneurons (C), CGRP immunoreactivity in dorsal horn (D) and adrenomedullin immunoreactivity in dorsal horn (E) of relapsing mice. In motoneurons CGRP was significantly increased ($p = 0.00181$; t test) whereas it was unchanged in dorsal horn fibers ($p = 0.21282$; t test), as it was adrenomedullin in dorsal horn fibers ($p = 0.23600$; t test). $n = 3$ for each group (ctr, rel). ctr = control; rel = relapsing.